

Production of soft e^+e^- Pairs in Heavy Ion Collisions at RHIC by Semi-coherent Two Photon Processes

Pilar Staig and Edward Shuryak

Department of Physics and Astronomy

Stony Brook University, Stony Brook NY 11794 USA

(Dated: October 26, 2018)

We calculate the contribution of the two photon production process into e^+e^- spectra, and compare the results with experimental data from the PHENIX detector at RHIC. We study the contribution given by “semi-coherent” kinematics, in which one photon is relatively hard and is incoherently emitted by participating protons, while another can be soft enough to be in a coherent domain.

I. INTRODUCTION

Thirty years ago one of us [1, 2] had suggested to use dileptons and photons as “penetrating probes” for dense hadronic matter created in ultrarelativistic heavy ion collisions, which – unlike hadrons – are observable from all stages of the collisions and thus can tell us what the initial hottest temperature reached can be. It is a very challenging task for experiments, as one has to remove hadronic backgrounds orders of magnitude larger than the photon or dilepton signal. And yet, over the years there were successful measurements, both at CERN SPS (muon pairs by NA50/NA60, electron pairs in CERES, photons in WA98) and RHIC (photons, muons and electrons in PHENIX, electrons in STAR). We will not go into details of these works, just make few general comments.

Already the above mentioned papers from 1970’s have singled out the so called intermediate mass dileptons (IMD’s), with the mass 1-3 GeV or between ϕ and J/ψ resonances, as the window for observing the thermal QGP radiation. More detailed predictions have been made in Ref. [4], where it has also been predicted that most of those pairs observed are *not* from charm decays, as was widely believed at the time. Only with successful completion of the NA60 experiment, with its sophisticated charm tracking, this collaboration had recently confirmed that they do indeed observe thermal radiation from QGP [5] and not just charm decays. For summary of other NA60 results see e.g.[7]: those include dileptons with small masses which come from resonances ρ mesons decaying in hadronic and near- T_c region. Although still far from being perfect, the existing theory provides a reasonable overall description of the NA60, see e.g. [3, 9]. Important recent observation of thermal photon radiation from hadronic gas and QGP has been also made by PHENIX collaboration [6], which is also in overall fair agreement with the current theory and the hydrodynamical picture of the collision.

And yet, some aspects of the experimental data at RHIC remain puzzling. Dilepton results from PHENIX show production rate of small mass $M \sim 500 MeV$ dileptons few times above theory predictions. Another puzzle is the presence of the so called “cold” component in the dilepton spectrum for $p_t < 500 MeV$, which is shown in

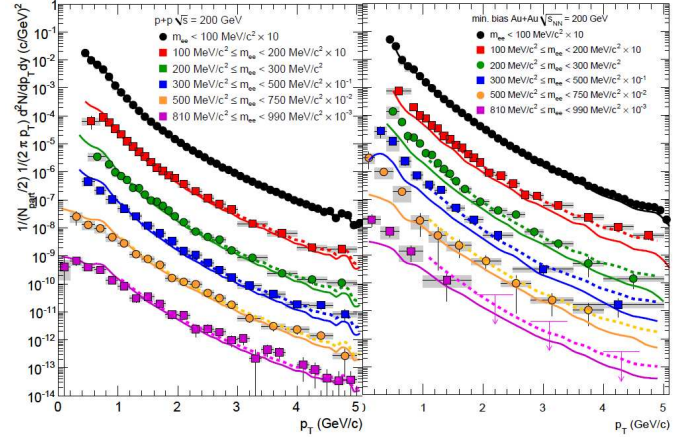


FIG. 1: (Color online) Acceptance corrected invariant e^+e^- yield versus total transverse momentum of the dilepton pair, for pp collisions (left) and AuAu collisions (right), from PHENIX publication [10]. The solid curves show the expectation from the sum of the so called hadronic cocktail contribution plus charm decays.

Fig.1. While the pp data (points in the l.h.s.) agree rather well with “hadronic cocktail” (curves), in AuAu data (r.h.s.) one finds systematic upward deviations of the data from from similar curves, at small p_t (the left side of the AuAu plot). If fitted with exponential, the data have a slope $T_{eff} \approx 100 MeV$, which is about twice smaller than the typical slope of the main “hot” component. What is especially strange about it is that this slope seems to be the same for different dilepton mass bins, see the three lowest curves on the right hand side in. This is in contrast to the “hot” component, which shows T_{eff} increasing with M , in good agreement with expectations based on hydrodynamical picture of expanding matter. It is a presence of such “cold” component which originally motivated us to have a look at some dilepton production mechanisms which are not included in the “standard” theory toolbox.

Small mass component is another puzzle, it has unusual centrality dependence.

Coherent two-photon processes are a well-known source of small mass and small p_t dileptons. Their basic theory had been developed already in 1930’s, when Lan-

dau and Lifshitz [11] calculated their total cross section for nuclear collisions using Weizsacker-Williams (WW) approximation. There have been extensive studies of the so called ultraperipheral processes in RHIC environment, for experimental results from STAR collaboration see [15]. As the name suggests, those processes take place at very large impact parameters $b > 2R$, at which no nuclear interactions take place. For electron pair production the characteristic b are related to the electron mass, and are thus very high. Theory development including all orders in $Z\alpha$ has been worked out in the last decade.

However the contribution of such processes at near-central collisions (when multiple hadronic production does happen) and for the kinematical range of p_t , M seen by PHENIX and NA60 has not to our knowledge been considered. This is what we are going to do in this work.

Additional motivation for looking at the two-photon processes comes from the standard relations between on-shell and slightly virtual photons γ^* , which are seen as small-mass dileptons. PHENIX has used such relations, relating dileptons with masses $M > 100 MeV$ with real photons. However, the two-photon collisions that we discuss do not obey it, producing only dileptons but not photons, and the question is how important are those in the kinematical range at hand.

II. THE FORMALISM

We use the Equivalent Photon Approximation (EPA)[12, 13] to determine the differential cross-section for the production of dileptons in Au-Au collisions. According to this method the effects of the electromagnetic fields from the moving nuclei can be replaced by the equivalent photon spectrum

$$dn_i = \frac{Z_i^2 \alpha q_{i\perp}^2 \left[F \left(q_{i\perp}^2 + \frac{w_i^2}{\gamma^2} \right) \right]^2 d^3 q_i}{\pi^2 \left(q_{i\perp}^2 + \frac{w_i^2}{\gamma^2} \right)^2 w_i} \quad (1)$$

where Z_i is the number of protons in the nucleus, $F(q^2)$ is the form factor of the nucleus charge, $q_{i\perp}$ is the transverse momentum of the photon and w_i is its energy. The differential cross-section for the gold-gold collision is then given by the product between the photon spectrum of each nucleus and the cross-section for the production of dileptons from a 2-photon collision:

$$d\sigma = \sigma_{\gamma\gamma} dn_1 dn_2 \quad (2)$$

$$(3)$$

which can be written in terms of the total transverse momentum $\vec{Q} = \vec{q}_1 + \vec{q}_2$ and integrated over \vec{q}_2 to give:

$$d\sigma = \sigma_{\gamma\gamma} \frac{(Z^2 \alpha)^2}{\pi^4} \frac{dq_{1z} dq_{2z}}{w_1 w_2} d^2 Q_{\perp} \int \frac{q_{2\perp}^2 \left[F \left(q_{2\perp}^2 + \frac{w_2^2}{\gamma^2} \right) \right]^2}{\left(q_{2\perp}^2 + \frac{w_2^2}{\gamma^2} \right)^2} \frac{(\vec{Q}_{\perp} - q_{2\perp}^{\vec{)}}^2 \left[F \left((\vec{Q}_{\perp} - q_{2\perp}^{\vec{)}}^2 + \frac{w_1^2}{\gamma^2} \right) \right]^2}{\left((\vec{Q}_{\perp} - q_{2\perp}^{\vec{)}}^2 + \frac{w_1^2}{\gamma^2} \right)^2} d^2 q_{2\perp} \quad (4)$$

Following [14] we see that the main contributions to the cross-section come from the regions where q_1 and q_2 are small (of the order of w_i/γ). If both of the momenta are small then the total transverse momentum would also have a small value and we are interested in studying the dilepton production for total transverse momentum up to about 0.7 GeV. This is why we work in a semi-coherent approach, in which from one of the nuclei we will get a coherent electric field, which will correspond to a photon with small transverse momentum, while the momentum from the other photon can have greater values. This means that in this case we won't be getting a coherent field from all the nucleus, but that the protons that compose it can have an individual effect. For this case, instead of using the form factor for a continuous charge distribution we will use the one coming from considering that the nucleus is composed of Z point particles.

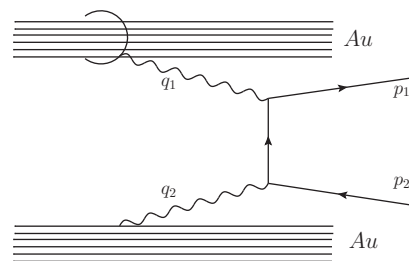


FIG. 2: (Color online) Dilepton production from a semi-coherent process.

For the case when $q_{2\perp} \ll Q_{\perp}$ we can approximate $\vec{Q}_{\perp} - q_{2\perp}^{\vec{}} \sim \vec{Q}_{\perp}$ so that we can take all the terms with Q_{\perp} from the integral, to get:

$$d\sigma = 2\sigma_{\gamma\gamma} \frac{(Z^2\alpha)^2}{\pi^4} \frac{\left[F\left(Q_\perp^2 + \frac{w_1^2}{\gamma^2}\right)\right]^2}{\left(Q_\perp^2 + \frac{w_1^2}{\gamma^2}\right)^2} \frac{dq_{1z}dq_{2z}}{w_1w_2} d^2Q_\perp$$

$$2\pi \int \frac{q_{2\perp}^3 \left[F\left(q_{2\perp}^2 + \frac{w_2^2}{\gamma^2}\right)\right]^2}{\left(q_{2\perp}^2 + \frac{w_2^2}{\gamma^2}\right)^2} dq_{2\perp} \quad (5)$$

The factor 2 in front comes from summing the two cases: when $q_{1\perp}$ is small and when $q_{2\perp}$ is small. Now, using

$$\begin{aligned} w_1 + w_2 &= m_t \cosh y \\ q_{1z} + q_{2z} &= m_t \sinh y, \end{aligned} \quad (6)$$

where $w_1 = \sqrt{Q_\perp^2 + q_{1z}^2}$, $w_2 = |q_{2z}|$ and $m_t = \sqrt{M^2 + Q_\perp^2}$, we make a change of variables from the photon longitudinal momenta q_{1z} and q_{2z} to the invariant mass M and the rapidity y . Then, putting $y = 0$ we get:

$$\begin{aligned} \frac{dq_{1z}dq_{2z}}{w_1w_2} &= \frac{M}{\left(1 + \frac{M^2}{\sqrt{4m_t^2Q_\perp^2 + M^4}}\right)^2} \left(1 + \frac{\sqrt{4m_t^2Q_\perp^2 + M^4}}{M^2}\right) \\ &\cdot \frac{4m_t^2}{M^2\sqrt{4m_t^2Q_\perp^2 + M^4}} dM dy \\ &= J(M, Q_\perp) dM dy \end{aligned} \quad (7)$$

Finally taking the integral over the invariant mass M , we get the cross-section as a function of the total transverse momentum Q_\perp and the rapidity y .

$$\begin{aligned} \frac{1}{2\pi Q_\perp} \frac{d^2\sigma}{dQ_\perp dy} &= \frac{4(Z^2\alpha)^2}{\pi^3} \frac{[F(Q_\perp)]^2}{Q_\perp^2} \frac{1}{2\pi} \int \int \sigma_{\gamma\gamma} \\ &\int \frac{q_{1\perp}^3 \left[F\left(q_{1\perp}^2 + \frac{w_1^2}{\gamma^2}\right)\right]^2}{\left(q_{1\perp}^2 + \frac{w_1^2}{\gamma^2}\right)^2} dq_{1\perp} dM d\phi_Q \end{aligned} \quad (8)$$

Since we work in the semi-coherent approach the cross-section $\sigma_{\gamma\gamma}$ is calculated using $q_1 = (w_1, \vec{Q}_\perp, q_z)$ and $q_2 = (q_z, \vec{0}, -q_z)$. This gives as a result $\sigma_{\gamma\gamma}(M, \vec{Q}_\perp, \phi_1, \theta_1)$. The angle ϕ_Q is integrated over 2π . The PHENIX detector covers $|\eta| < 0.35$ and a total of 180° in azimuth, but the data has been acceptance corrected to include electrons and positrons from all directions. The only restriction that we must impose is due to the single track acceptance condition that $p_\perp > 0.2 \text{ GeV}$.

III. FORM FACTORS

The charge distribution of the nucleus can be well parameterized by the Woods-Saxon expression

$$\rho(r) \propto \frac{1}{e^{\frac{r-R}{a}} + 1} \quad (9)$$

with two parameters, the nuclear radius R (6.55 fm for Au) and the width of the nuclear edge which is typically about $a = 0.5$ fm [16]. Starting from this charge distribution it is not possible to get an analytical expression for the form factor, but the integrals of the fourier transformation can be done numerically, to get a form factor of the shape seen in FIG. 3.

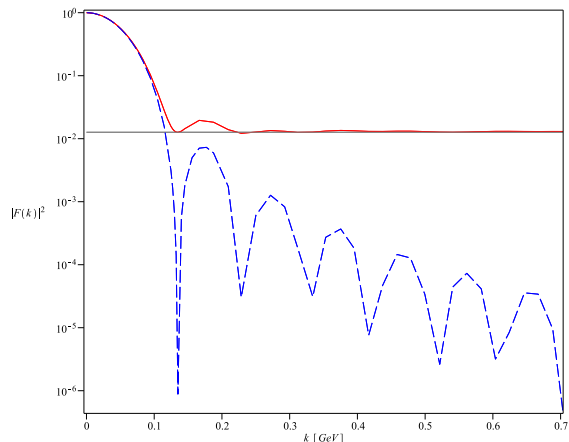


FIG. 3: (Color online) The square of the form factors plotted on a logarithmic scale. The (blue) dashed line corresponds to smooth Woods-Saxon charge distribution, the (red) continuous line corresponds to resolved discrete protons (but not quarks), as explained in the text.)

As it has been stated previously, we are working in a semi-coherent approach. This means that while one of the photons is soft and thus sees the nucleus as a uniform charge distribution (with the Woods-Saxon shape), the other can have a large transverse momenta and thus resolve individual protons. For this later case we will use the picture of instantaneously frozen nucleons, which just means that at any given moment the protons are randomly distributed in the nucleus according to some weight and frozen in these positions x_m , where x is in the direction where the momentum Q_\perp is directed. So the form factor can be written as:

$$\begin{aligned} F(k) &= \frac{1}{Z} \int e^{ikx} \sum_{m=1}^Z \delta(x - x_m) dx \\ &= \frac{1}{Z} \sum_{m=1}^Z e^{ikx_m} \end{aligned} \quad (10)$$

In the amplitude we have the square of the form factor, so what we need is:

$$|F(k)|^2 = \frac{1}{Z^2} \left[Z + 2 \sum_{m=1}^Z \sum_{n=1}^{m-1} \cos(k(x_m - x_n)) \right] \quad (11)$$

In Fig.3 we plot this quantity and compare it to the form factor from the Woods-Saxon distribution. We see that for small momenta they are almost the same but as the momentum is increased the Woods-Saxon one goes to zero while the one for the point charges doesn't. This happens because at small momentum the nucleus is seen as a whole and all the protons are acting coherently. From eqn.11 we see that for $k(x_m - x_n) \ll 1$ the square of the form factor $|F(k)|^2 \sim 1$, which means that the nucleus acts coherently for momenta up to about $k \sim 1/R$ but as the momentum increases, the contributions from the different protons start to add up incoherently until, at high momentum, all the different phases cancel out and we are left only with protons interacting individually with other protons. So the form factor for the Woods-Saxon charge distribution, or for any other uniform distribution which may represent the nucleus, is only valid for low momenta but stops working as the momentum increases, due to the fact that the nuclear substructure can be discerned at high enough momenta.

IV. RESULTS

In order to present our results in a way that allows them to be compared with data from RHIC, we will study the invariant yield which is given by:

$$\begin{aligned} Yield &= \frac{1}{N_{part}/2} \frac{1}{2\pi Q_{\perp}} \frac{d^2 N}{dQ_{\perp} dy} \\ &= \frac{1}{N_{part}/2} \frac{1}{\sigma_{total}} \frac{1}{2\pi Q_{\perp}} \frac{d^2 \sigma}{dQ_{\perp} dy} \end{aligned} \quad (12)$$

where $\sigma_{total} \sim 4\pi R^2 \sim 1.4 \cdot 10^4 [GeV^{-2}]$. The data from PHENIX correspond to a minimum bias situation, so the collisions considered have centrality in the range 0 – 92% which corresponds to $N_{part} = 109$ [17]. Note that very peripheral, elastic and diffractive events, both in terms of pion production and nuclear physics, are not included: however those still can generate dileptons.

It is also important to notice that the “acceptance corrected” simply means the geometric acceptance of the pair. Separately from this, the detector has a single track acceptance condition for the transverse momentum of each lepton

$$p_{\perp} > p_{min} = 0.2 GeV \quad (13)$$

needed for them to reach the detector in the current magnetic field. The reported cross section [10] still is under this condition. This translates into a truncation

for small pair transverse momentum Q_{\perp} , for invariant masses smaller than $0.4 GeV$.

In our calculation, if the electron mass is neglected, the $\gamma\gamma \rightarrow e^+e^-$ cross section has collinear singularity, when the leptons move along the directions of the photons. The experimental condition (13) supersedes the cutoff coming from finite electron mass: thus we apply the same single track acceptance condition in our calculations.

Since we work in a semi-coherent approach, we keep the transverse momentum of one of the photons small, with an upper bound given by $min(Q_{\perp}, 1/R)$, where the whole nucleus acts coherently. In principle, the lower bound on $q_{2\perp}$ is extremely small, related to the electron mass, and ultraperipheral collisions with very large impact parameters would be included in the result. However, as we mentioned earlier, these are not included in the PHENIX data, so in order to compare it with our results we had to restrict the minimum value of $q_{2\perp}$. Fortunately, the integral over this variable is logarithmic, so we need only order-of-magnitude estimate of its lowest value. Roughly speaking, PHENIX only includes collisions in which two nuclei directly touch each other, or $b < 2R$. The strongest and the weakest electric fields of one nuclei inside the disc of the other corresponds to distances from R to to $3R$. The latter distance we thus associate with the cutoff on the minimal $q_{2\perp}$ value. This is needed only for the “softest” photon: the other one has large $q_{1\perp}$, by kinematics, and thus corresponds to field fluctuations inside the disk of the nucleus 1.

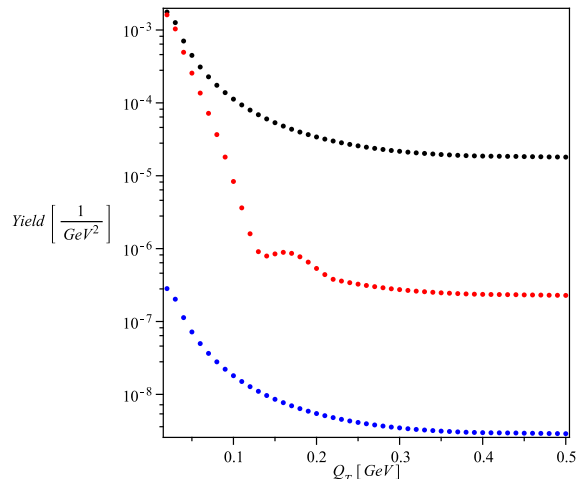


FIG. 4: (Color online) Yield versus total transverse momentum. From top to bottom: coherent, semi-coherent, totally incoherent.

In Fig.4 we show our results for the yield as a function of the total transverse momentum Q_{\perp} . As expected, we see that for small momenta, while it is in the coherent regime, the differential cross-section is large, but when the momentum is increased the yield decreases. We compare the semi-coherent case with a totally coherent case, in which we took the nuclei to be point particles of charge Ze , and with the totally incoherent case, when

we ignore all interferences and consider collisions of protons each on each. We see that the semi-coherent case lies in between. It starts, for low transverse momentum, overlapping with the totally coherent curve and as the momentum increases it drops, but it never reaches the incoherent curve because we let one of the photon transverse momentum be small, so that one of the nuclei is always giving a coherent contribution.

For different mass bins the shape of the yield as a func-

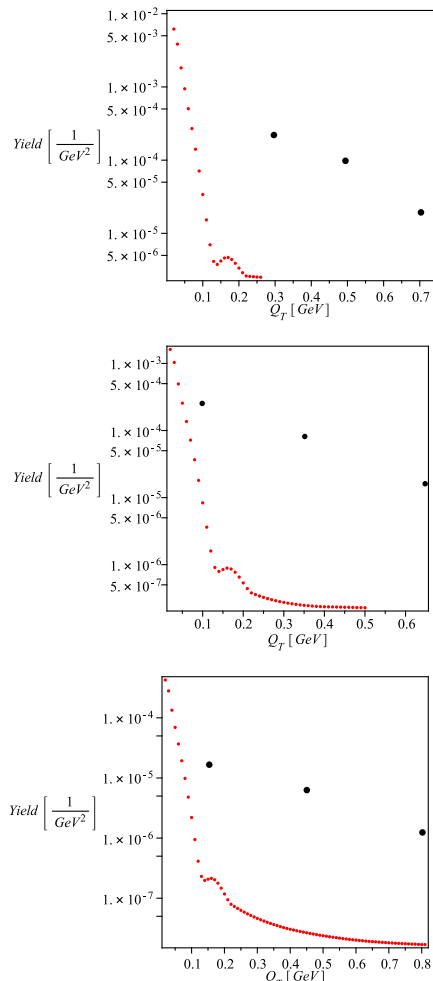


FIG. 5: (Color online) Yield versus total transverse momentum for different invariant mass ranges. Open (red) symbols are the two-photon contribution, compared with PHENIX data (black closed points, taken from Fig.1). From top to bottom: $M=300-500, 500-750, 810-990$ MeV. For the lower mass range the single track acceptance was relaxed from $p_{\perp} > 0.2$ to $p_{\perp} > 0.1$ in our calculations.

tion of the transverse momentum is the same. In Fig.5 the yield for three mass ranges is presented and it can be seen that the lowest the invariant mass the higher the yield, as expected. In order to include the upper plot, which is in the mass range $300 - 500$ MeV, the single track acceptance constraint has been relaxed to $p_{\perp} > 0.1$ GeV for this case. We compare our results with experimental data from PHENIX, which is given by the filled black dots in the plot. We see that the contribution

from the semi-coherent production of dileptons is about two orders of magnitude smaller than the experimental results. From this we conclude that in the momentum ranges explored the dilepton production from two photon collisions doesn't contribute significantly to the total production of electron-positron pairs in Au-Au collisions, but this mechanism is important for smaller transverse momenta, when the two photons are a result of the coherent interaction of the nuclear electromagnetic fields.

The applicability of the EPA requires that the photon transverse momenta are small in respect to all other invariants. Therefore, in Fig.5 we stop our curves when Q_{\perp}^2 reaches the dilepton mass squared, where this condition is not fulfilled. Note however that in the region where the two-photon production has chances to be observed, this condition is rather accurate.

For completeness, we also calculated a contribution of this semi-coherent approach for the LHC energy range, where $\gamma \sim 3400$. In the unrestricted case, when the photon with small transverse momentum is in the range $0 < q_{2\perp} < \min(Q_{\perp}, 1/R)$, the integral over $q_{2\perp}$ gives the usual $\ln(\frac{\gamma q_{2\perp}^{max}}{w})$, so the increase in gamma implies a further "ultra-peripheral" enhancement of the process. Using the ALICE detector acceptance of $|\eta| < 0.9$ with full range in azimuth and a single track acceptance of $p_{\perp} > 0.1$ [18] and allowing $q_{2\perp}$ to be integrated in the region just described, there is an enhancement of one order of magnitude in comparison to our results for the PHENIX acceptance and with $q_{2\perp}$ in the same range. However, when we restrict $q_{2\perp}$ to be between $1/3R$ and $\min(Q_{\perp}, 1/R)$ and in this way don't consider ultra-peripheral collisions, the results for the yields that we calculate for PHENIX and ALICE are very similar and the small difference between them (about a factor 2 for small transverse momentum) is due to the greater acceptance of the latter and also to the different elements used ($Z=79$ for RHIC and $Z=82$ for LHC).

V. RESOLVING QUARKS

To end this study of dilepton production in heavy ion collisions, we consider the structure of the nucleons, this is we resolve partons such that, as before, from one of the nuclei we get a coherent contribution (small momenta) while from the other one we get the effect from partons acting individually. To determine the parton contribution we must turn to use the parton distribution functions (PDF's).

The nucleons are composed of quarks and gluons and the probability that a given nucleon contains a constituent particle with x momentum fraction of the total momentum of the nucleon corresponds to $f_i(x)dx$, where the functions f_i are the PDF's for the i type constituent ($i = u, \bar{u}, d, \bar{d}, s, \bar{s}, c, \bar{c}, b, \bar{b}, t, \bar{t}, gluon$) for a proton.

In our calculations we use data from the CTEQ collaboration [19] and we only consider the three lightest quarks: u and d valence quarks and u,d and s sea quarks.

x_{min}	u	\bar{u}	u_v	d	\bar{d}	d_v	s
0.01	2.452	0.763	1.690	1.703	0.864	0.839	0.521
0.0025	4.305	2.386	1.918	3.475	2.505	0.970	1.775
0.001	5.249	3.253	1.996	4.390	3.377	1.013	2.451

TABLE I: (Color online)Number of quarks calculated by integrating the PDF's from CTEQ from different x_{min} .

To determine the number of each kind of quark present in a nucleon we integrate the corresponding PDF's from x_{min} to 1, some examples can be seen in table I.

In order to consider all the partons that are capable of emitting a photon of energy w , we take x_{min} to correspond to that energy. Since in Au-Au collisions at RHIC the typical center of mass energy per nucleon is of 100 GeV, $x_{min}=0.01$ implies that all the partons that can emit a photon of $w = 1GeV$ are taken into account. We consider partons from protons and neutrons, the PDF's for both types of nucleon are related by isospin symmetry so for the neutrons the up and down quarks are interchanged with respect to protons.

We use $x_{min} = 0.0025$ to calculate the number of each kind of quark present in a gold nucleus and then we proceed as before, working in the instantaneously frozen picture. We randomly select the positions of the quarks in the nucleus to determine

$$F(k) = \frac{\frac{2}{3} \sum_{i=1}^{n_u} e^{ikx_{u_i}} - \frac{2}{3} \sum_{i=1}^{n_{\bar{u}}} e^{ikx_{\bar{u}_i}} - \frac{1}{3} \sum_{i=1}^{n_d+n_s} e^{ikx_{d_i}} + \frac{1}{3} \sum_{i=1}^{n_{\bar{d}}+n_{\bar{s}}} e^{ikx_{\bar{d}_i}}}{\frac{2}{3}(n_u - n_{\bar{u}}) - \frac{1}{3}(n_d - n_{\bar{d}}) - \frac{1}{3}(n_s - n_{\bar{s}})}$$

then this quantity is squared and averaged over different quark configurations. The result is plotted on the left side in Fig.6 and compared to the previous case when we resolved only up to nucleons. For small momenta the form

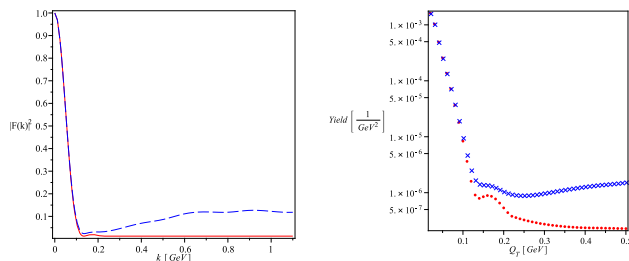


FIG. 6: (Color online)LEFT:Comparison between form factors. Continuous line:resolving up to protons, dashed line:resolving up to partons. RIGHT:Yield versus total transverse momentum for an invariant mass range of 500-750 MeV. Upper curve: resolving up to partons. Lower curve: resolving up to protons.

factor is as before, and the nucleus gives a coherent contribution, but for large momenta, when the value comes from the incoherent contributions of individual particles, the result obtained from resolving up to partons is about one order of magnitude larger than when resolving only up to protons, because the number of participating particles is increased since we not only consider the valence quarks from the proton but also the sea quarks and all the quarks from the neutrons.

In Fig.6 we also present the comparison for the yield as a function of total transverse momentum between the two cases that we have studied: resolving up to protons and resolving up to partons. We see that for momenta larger than 0.1 GeV, the contribution to the dilepton production process is larger when we take into account the nucleon structure, but it is still orders of magnitude below the experimental data.

VI. SUMMARY

We studied the production of dileptons in heavy ion collisions using the two-photon mechanism, in the double effective photon approximation. It is well known since 1930's [11] that for low momenta the contribution from both nuclei is coherent and in this case the cross section for the process is proportional to $(Z\alpha)^4$. Our main interest was to look at the regime in which this coherence is lost.

Although our original motivation was to explain the RHIC puzzles, we learned (relatively early in the calculation) that the two-photon mechanism unfortunately cannot explain any of them. Yet we persisted and completed this calculation, for two reasons.

One is that with relatively minor modification of the PHENIX experimental condition – in particular with reduction of the magnetic field – the dilepton from the two-photon mechanism would become detectable and maybe even dominant. Thus it would be beneficial to identify and study those, in next RHIC runs. It would not require significant expense, as we speak about quite large cross sections.

Another reason is a theoretical curiosity: what exactly happens with the two-photon cross section when the coherence is lost. We found that when it happens, the cross section is dominated by a “semi-coherent” regime, in which the momentum of one of the photons remains small enough to be represented as a coherent field of one of the nuclei, while allowing the other photon to have larger momentum and resolve individual particles, protons or even quarks. We have shown in this paper that the semi-coherent approach gives a greater contribution than the totally incoherent case, while still allowing the dilepton pair to have relatively large total transverse momentum.

We studied two cases, first resolving only up to protons and then resolving them into charged partons (quarks). By comparing both results we see that the larger the number of particles that are resolved, the greater the contribution. Unfortunately, such increase – by almost one order of magnitude – is not enough to explain the total dilepton spectrum observed at RHIC.

However, there can be similar semi-coherent regime for other processes in QCD, especially at $Q \sim 1GeV$. Traditionally, few-GeV momenta transfer is seen as a domain of parton model, with its treated via completely incoherent PDF's and cross sections for hard processes.

And yet, even for gluons, people introduced “color glass” fields collectively generated by many hard partons [20]. The so called “ridge” phenomenon, recently discovered by STAR collaboration [21], is presumably due to early local large-scale fluctuation of color field [22]. A collision of such fields with the usual incoherent partons can presumably generate a QCD analog of “semi-coherent” processes we studied above.

VII. ACKNOWLEDGEMENTS

We thank Tony Baltz for a useful discussion of the form factors. The work is partially supported by the US-DOE grants DE-FG02-88ER40388 and DE-FG03-97ER4014.

-
- [1] E. V. Shuryak, Phys. Lett. B **78**, 150 (1978) [Sov. J. Nucl. Phys. **28**, 408.1978 YAFIA,28,796 (1978 YAFIA,28,796-808.1978)].
- [2] E. V. Shuryak, Phys. Rept. **61**, 71 (1980).
- [3] H. van Hees and R. Rapp, Nucl. Phys. A **806**, 339 (2008) [arXiv:0711.3444 [hep-ph]].
- [4] R. Rapp and E. V. Shuryak, Phys. Lett. B **473**, 13 (2000) [arXiv:hep-ph/9909348].
- [5] R. Arnaldi *et al.* [NA60 Collaboration], “Thermal Dimuon Emission in In-In at the CERN SPS,” arXiv:0806.0577 [nucl-ex].
- [6] A. Adare *et al.* [PHENIX Collaboration], arXiv:0804.4168 [nucl-ex].
- [7] R. Arnaldi *et al.*, arXiv:0904.3186 [hep-ex].
- [8] K. Dusling and I. Zahed, Nucl. Phys. A **825**, 212 (2009) [arXiv:0712.1982 [nucl-th]].
- [9] K. Dusling and I. Zahed, Phys. Rev. C **80**, 014902 (2009) [arXiv:hep-ph/0701253].
- [10] and A. Adare [PHENIX Collaboration], arXiv:0912.0244 [nucl-ex].
- [11] L. D. Landau and E. M. Lifschitz, Phys. Z. Sowjetunion **6**, 244 (1934).
- [12] V.B. Berestetskii, E.M. Lifshitz, L.P. Pitaevskii, *Relativistic Quantum Theory*, Pergamon Press (First Edition, 1974)
- [13] J.D. Jackson, *Classical Electrodynamics*, Wiley (Third Edition,1999)
- [14] V. M. Budnev, I. F. Ginzburg, G. V. Meledin and V. G. Serbo, Phys. Rept. **15**, 181 (1975).
- [15] B. I. Abelev *et al.* [STAR Collaboration], Phys. Rev. C **77**, 034910 (2008) [arXiv:0712.3320 [nucl-ex]].
- [16] G. Fricke *al.*, Atomic Data and Nuclear Data Tables **60**, 177 (1995).
- [17] T. Dahms, arXiv:0810.3040 [nucl-ex].
- [18] R. Schicker [ALICE Collaboration], Nucl. Phys. Proc. Suppl. **179-180**, 196 (2008) [arXiv:0807.1472 [physics.ins-det]].
- [19] J. Pumplin, D. R. Stump, J. Huston, H. L. Lai, P. M. Nadolsky and W. K. Tung, JHEP **0207**, 012 (2002) [arXiv:hep-ph/0201195].
- [20] L. D. McLerran and R. Venugopalan, Phys. Rev. D **49**, 2233 (1994) [arXiv:hep-ph/9309289].
- [21] M. Daugherty (for the STAR coll.), Anomalous centrality variation..., QM08, J.Phys.G.Nucl/Part.Phys. **35** (2008) 104090
- [22] A. Dumitru, F. Gelis, L. McLerran and R. Venugopalan, Nucl. Phys. A **810**, 91 (2008) [arXiv:0804.3858 [hep-ph]].